Articles

Submicron Patterning of Iron Nanoparticle Monolayers for Carbon Nanotube Growth

Eric W. Wong,* Michael J. Bronikowski, Michael E. Hoenk, Robert S. Kowalczyk, and Brian D. Hunt

Jet Propulsion Laboratory, California Institute of Technology, Pasadena, California

Received July 23, 2004. Revised Manuscript Received October 27, 2004

We describe a method to reliably pattern monolayers of iron nanoparticle (FeNP) colloids into submicron features for growth of single-walled carbon nanotubes (SWNTs) by chemical vapor deposition. Our process results in very clean patterns that are readily imaged by atomic force microscopy, which has allowed the observation of nanoparticle size evolution before and after high-temperature nanotube growth. For our growth conditions, SWNTs grew only from nanoparticles smaller than ∼5 nm high. At the high growth temperature of 850 °C, nanoparticle sintering was clearly evident and had important effects on nanotube yield from the FeNP catalyst. The nanoparticle sintering and growth are drastically accelerated by brief reduction in H_2, resulting in nanoparticles that were too large to catalyze SWNT growth. The results suggest that if ultimate control over SWNT diameters is to be achieved from patterned nanoparticle catalysts, it will be critical to control nanoparticle aggregation and sintering during SNWT growth.

Introduction

In the brief decade since their discovery carbon nanotubes have inspired a tremendous amount of research into understanding their unique properties as well as their potential technological applications.[1] Single-walled nanotubes (SWNTs) have shown promise in high performance electronic applications such as chemical sensors,[2,3] nonvolatile memory,[4] and electron field emission sources.[5,6] To realize their potential as nanodevices, there still remains the hurdle of controlling the growth or placement of a specific type (i.e., semiconducting or metallic) and size (diameter and length) of nanotube at a desired location and orientation on a chip. A great deal of progress has been made beyond the many fascinating devices made by the laborious process of first finding a desired nanotube on a substrate and then patterning electrodes to fabricate the final nanotube device. Control over the direction of nanotube growth has been achieved along the direction of gas flow[7] or applied electric field.[8] Large scale integration of arrays of nanotube devices onto a single chip has been achieved by growth of SWNTs from patterned nanotube catalysts positioned on pre-defined electrodes.[9,10] While nanotubes bridge most of the electrode pairs, there is little control over the type of nanotubes, the number of nanotubes, and the direction of growth. To improve control over nanotube growth for nanoscale device integration, further understanding of the parameters that determine nanotube growth is required, as well as new methods for patterning nanoscale catalysts tailored for the growth of specific nanotubes.

There has been a great deal of progress in understanding the various factors that govern single-walled nanotube growth, including the catalyst composition, particle size, reactive gas composition, pressures, and temperatures.[11] SWNTs have been grown from a variety of catalysts such as iron nanoparticles,[12−16] Fe/Mo[9,17,18] or Co/Mo[19] on supported on alumina particles, and evaporated Fe.[20] Controlling

* To whom correspondence should be addressed. E-mail: Eric.W.Wong@jpl.nasa.gov.

(1) Baughman, R. H.; Zakhidov, A. A.; de Heer, W. *Science* **2002**, *297*, 787.
(2) Qi, P.; Vermash, O.; Grecu, M.; Javey, A.; Wang, Q.; Dai, H. *Nano Lett.* **2003**, *3*, 347.
(3) Besteman, K.; Lee, J.-O.; Wiertz, F. G. M.; Heering, H. A.; Dekker, C. *Nano Lett.* **2003**, *3*, 727.
(4) Rueckes, T.; Kim, K.; Joselevich, E.; Tseng, G. Y.; Cheung, C.-L.; Lieber, C. M. *Science (Washington, D. C.)* **2000**, *289*.
(5) Fan, S.; Chaplin, M. G.; Franklin, N. R.; Tombler, T. W.; Cassell, A. M.; Dai, H. *Science (Washington, D. C.)* **1999**, *283*, 512.
(6) Wang, Q. H.; Setlur, A. A.; Lauerhaas, J. M.; Dai, J. Y.; Seelig, E. W. *Appl. Phys. Lett.* **1998**, *72*, 2912.
(7) Huang, S.; Maynor, B.; Cai, X.; Liu, J. *Adv. Mater.* **2003**, *15*, 1651.
(8) Zhang, Y.; Chang, A.; Cao, J.; Wang, Q.; Kim, W.; Li, Y.; Morris, N.; Yenilmez, E.; Kong, J.; Dai, H. *Appl. Phys. Lett.* **2001**, *79*, 3155.
(9) Kong, J.; Soh, H. T.; Cassell, A. M.; Quate, C. F.; Dai, H. *Nature* **1998**, *395*, 878.
(10) Franklin, N. R.; Li, Y.; Chen, R. J.; Javey, A.; Dai, H. *Appl. Phys. Lett.* **2001**, *79*, 4571.
(11) Moisala, A.; Nasibulin, A. G.; Kauppinen, E. I. *J. Phys.: Condens. Matter* **2003**, *15*, S3011.
(12) Li, Y.; Liu, J. *Chem. Mater.* **2001**, *13*, 1008.
(13) Li, Y.; Mann, D.; Rolandi, M.; Kim, W.; Ural, A.; Hung, S.; Javey, A.; Cao, J.; Wang, D.; Yenilmez, E.; Wang, Q.; Gibbons, J. F.; Nishi, Y.; Dai, H. *Nano Lett.* **2004**, *4*, 317.
(14) Cheung, C. L.; Kurtz, A.; Park, H.; Lieber, C. M. *J. Phys. Chem. B* **2002**, *106*, 2429.
(15) Homma, Y.; Yamashita, T.; Finnie, P.; Tomita, M.; Ogino, T. *Jpn. J. Appl. Phys.* **2002**, *41*, L89.
(16) Choi, H. C.; Kundaria, S.; Wang, D.; Javey, A.; Wang, Q.; Rolandi, M.; Dai, H. *Nano Lett.* **2003**, *3*, 157.

10.1021/cm048795m CCC: $30.25
Published on Web 12/21/2004

nanotube growth will be essential for fabricating nanotube-based devices. The various growth methods have used methane or other hydrocarbons to grow single-walled nanotubes from dispersed metal or metal oxide catalysts at high temperature (usually ~800−1000 °C), often with hydrogen to minimize the amount of amorphous carbon that is produced. One study has found that SWNTs grow in a narrow window of H_2 to CH_4 ratios, with growth being suppressed by too much hydrogen or overwhelmed by pyrolytic growth (i.e., no SWNTs) with insufficient hydrogen. The growth substrates have also proven to be critical in obtaining good SWNT growth. Growing SWNTs on metallic electrodes has proven challenging because these electrodes poison the catalysts. This is understandable since iron easily forms alloys with many of the electrode materials that have been employed for device fabrication. To alleviate this difficulty, controlled SWNT growth has been achieved on electrodes by using alumina-supported catalysts or oxide barrier layers to protect the catalyst from the underlying electrode.[21]

An important issue is how the nanotube diameter depends on the size of a catalyst particle. Some mechanistic studies have shown a close correlation between catalyst size and the resulting nanotube diameter.[12,14,22] In one study, the mean nanotube diameters of 3, 7, and 12 nm closely corresponded to those of iron nanoparticles that were synthesized with monodisperse diameters of 3, 9, and 13 nm,[14] respectively. Interestingly, achieving the desired nanotube diameter required increasing the partial pressure of hydrocarbon with increasing particle size, where too small a partial pressure resulted in small nanotube diameters for all particle sizes. It has also been suggested that the catalyst particles can evolve during the course of a growth process. In fact, the same alumina-supported Fe/Mo-based catalysts used to make SWNTs were initially used to grow multiwalled nanotubes (MWNTs) in a process requiring an inductive heating period in H_2 to grow sufficiently large catalytic particles.[17] Characterization of the catalytic nanoparticles is made difficult in this type of catalyst because of the preponderance of the supporting alumina particles. It was also reported that iron nanoparticles decreased in population during CVD because of evaporation or sintering[23] and could fuse into larger particles that grow thick MWNTs.[15] While controlling the starting size of nanoparticles is important for determining the SWNT diameters, it is essential to understand how aggregation and sintering during CVD affects SWNT growth.

We report a method to reliably pattern monolayers of iron nanoparticles into submicron features. We use atomic force microscopy (AFM) to characterize the sintering of nanoparticles within patterned regions and show how controlling the fusing of nanoparticles is critical to obtaining good SWNT growth. While it is has been possible to grow SWNTs from patterned regions of a few micrometers, the growth substrates have been difficult to characterize because the alumina-supported catalysts form uneven mounds with varying amounts of catalyst.[9] By another method, iron nanoparticles were successfully formed after first patterning $FeCl_3$, but control over particle size (2.2 ± 0.9 nm) and monodispersity was limited.[16] Our method patterns pre-synthesized Fe nanoparticles stabilized with oleic acid into regions as small as 200 nm, allowing the nanoparticle diameters to be controlled prior to patterning. We have found that PMMA resists give superior control over the amount of catalyst deposited and result in much cleaner liftoffs than photoresists which have been used previously to pattern iron nanoparticles.[7] Additionally, we have explored how three parameters determine the degree of nanoparticle sintering and impact the SWNT yield: (1) the order of gas introduction, (2) the annealing time, and (3) the gas flow near the sample.

Experimental Section

The iron nanoparticles used in these studies were synthesized similar to a published procedure.[24] The primary difference in our procedure is that we omitted the oxidation to Fe_2O_3, so that our FeNPs are composed of an Fe core with a native Fe_2O_3 shell. The distribution of nanoparticle diameters was 5.8 ± 2.0 nm as determined by transmission electron microscopy (TEM) using an Akisha EM-002b at 100 kV. The distribution was made intentionally wide to maximize the probability of having catalytic particles, although they can be made with narrow size distributions.[24] Iron nanoparticles were patterned into 1-μm dot regions onto oxidized silicon substrates using 3000-Å-thick PMMA (MicroChem, 950 K, 4% in chlorobenzene) baked at 170 °C or 1.4-μm-thick AZ5214 photoresist (Clariant) baked at 95−105 °C. After patterning holes into the resist, a typical procedure begins with descumming the bottom of the holes with an oxygen plasma (100 W, 0.5 Torr O_2, 1 min.) This step was essential for reliable sticking of the FeNPs to the patterned regions. A few drops of FeNPs in a hexane solution (1.5 mg/mL)[25] is deposited onto the resist and allowed to sit for 5−10 s, adding a drop of hexane as needed to avoid drying. This allows the FeNPs to self-assemble onto the substrate at the bottom resist holes. Without allowing the substrate to dry, it is spun to 2000 rpm while rinsing with hexane (~1−2 mL) and then dried by heating at 95 °C for 5−10 min. The resist is removed by immersing the substrate in acetone for 2 min followed by a brief acetone rinse. The liftoff was characterized by AFM using a DI Nanoscope III using silicon probes in TappingMode. Figure 1A shows an AFM image of an array of 1-μm dots produced using a PMMA resist after the resist strip and oxygen plasma cleaning for 3 min. There are several things to note. The FeNPs stick very well and allow for facile AFM imaging as also shown in the high-resolution image in Figure 1B. The FeNPs are well packed as individuals and as small agglomerates of 3−4 particles. Close packed hexagonal structures are short range, extending only over a few nanoparticle diameters, but this is expected given the wide

(17) Snyder, C. E.; Mandeville, H. W.; Tennent, H. G.; Truesdale, L. K.; Barber, J. J. Carbon Fibrils; Hyperion Catalysis International. U.S. Patent 5,707,916, 1998.
(18) Cassell, A. M.; Raymakers, J. A.; Kong, J.; Dai, H. *J. Phys. Chem. B* **1999**, *103*, 6484.
(19) Alvarez, W. E.; Kitiyanan, B.; Borgna, A.; Resasco, D. E. *Carbon* **2001**, *39*, 547.
(20) Nerushev, O. A.; Dittmar, S.; Morjan, R.-E.; Rohmund, F.; Cambell, E. E. B. *J. Appl. Phys.* **2003**, *93*, 4185.
(21) Seidel, R.; Liebau, M.; Duesberg, G. S.; Kreupl, F.; Unger, E.; Graham, A. P.; Hoenlein, W. *Nano Lett.* **2003**, *3*, 965.
(22) Li, Y.; Kim, W.; Zhang, Y.; Rolandi, M.; Wang, D.; Dai, H. *J. Phys. Chem. B* **2001**, *105*, 11424.
(23) Choi, H. C.; Kim, W.; Wang, D.; Dai, H. *J. Phys. Chem. B* **2002**, *106*, 12362.
(24) Hyeon, T.; Lee, S. S.; Park, J.; Chung, Y.; Na, H. B. *J. Am. Chem. Soc.* **2001**, *123*, 12798.
(25) The solution is stable for over 9 months but is made unstable by further dilution in hexane. The dried FeNPs could be easily re-dispersed in hexane and used for SWNT growth after two years.

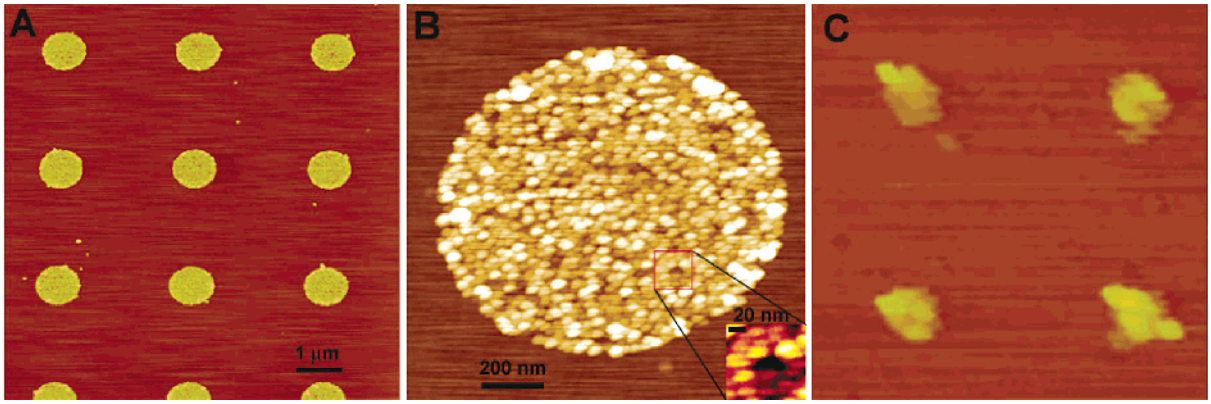

Figure 1. Iron nanoparticles patterned into uniform monolayer dots with average heights of 5.7 nm. The AFM height images show (A) a low magnification image of a dot array, (B) a high-resolution image of a single dot with inset of single nanoparticles, and (C) iron nanoparticles patterned into 200-nm-diameter dots. The images were obtained using a Digital Microscopes III in tapping mode using a Si probe at 150 kHz.

size distribution. Analysis of the image shows a height distribution centered at 5.7 ± 1.8 nm which roughly corresponds to a monolayer of nanoparticles and is consistent with TEM measurements. Closer examination shows that voids without FeNPs and bilayers each make up ~%15 of the dot area while a monolayer covers the remaining 70% of the area. Thus, the overall composition of the dot is roughly a monolayer of iron nanoparticles. Also, the substrate surrounding each dot is very clean and the pattern formation is excellent across a 1-cm chip. This rinsing procedure is important for obtaining regions between the dots that are free from FeNPs. Using this method, FeNPs have been patterned reliably into 200-nm dots (formed by e-beam lithography) as shown in Figure 1C. It was possible to obtain FeNP patterned into dots using AZ5214 photoresist; however, the regions between dots always contained residual FeNPs, the amount of which was very sensitive to small variations in deposition and rinsing procedures.[26] Other photoresists were not tested.

The clean patterning of monolayers of FeNPs depends on the oleic acid capping of the nanoparticles. The oleic acid capping allows the nanoparticles to form a stable colloid in hexane. The amount of FeNPs that is deposited into the resist holes is determined by self-assembly onto the substrate rather than by sedimentation, as would be the case with an unstable colloid such as the supported alumina catalysts. Rinsing with hexane removes excess nanoparticles and leaves approximately a monolayer in the holes. The oleic acid also renders the nanoparticles highly insoluble in acetone and causes them to stick to the substrate during liftoff.

The substrates patterned into 1-μm dots of FeNPs were used for the SWNT growth studies. Since patterning was consistently uniform and produced dots with roughly a monolayer of FeNPs, SWNT yields from different growth runs could be easily compared. The growths were performed using a tube furnace with a 2-in.-diameter quartz tube. All the growths were done at 850 °C using CH_4 (1500 sccm) and H_2 (50 sccm) at a pressure of 780 Torr. Substrates were ramped to 850 °C in 15 min under argon and 10 min growths were initiated by simultaneously turning the argon off and the reactive gases on. As will be discussed, minor changes in the order and timing of when the reactive gases are initiated are critical for determining the degree of particle sintering and the resulting SWNT yield.

(26) PMMA that was photopatterned via a top layer of AZ5214 resulted in clean liftoff only after completely removing the AZ5214 after defining the holes in the PMMA. Removal of the AZ5214 top layer was not necessary if a 15-nm titanium layer separated the bottom PMMA and top AZ5214. In this case, the titanium layer came off as a single sheet, thereby removing residual FeNPs. However, liftoff using the Ti barrier layers was only reliable for isolated dots and not closely spaced arrays.

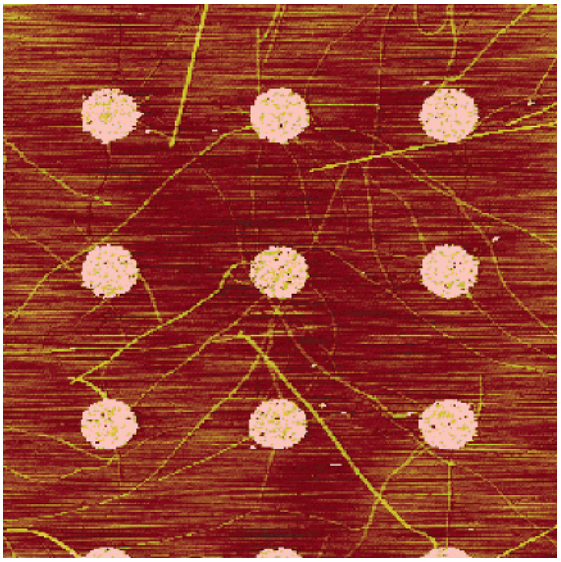

Figure 2. SWNTs grown from patterned FeNP dots. The AFM image was obtained after *growth 1* which has no H_2 pretreatment. The average heights of the 1-μm-diameter catalyst dots and SWNTs are 4.8 and 1.1 nm, respectively.

Results and Discussion

For the FeNPs, the highest yield of SWNTs was obtained by initiating the CH_4 and H_2 flows at the same time (*growth 1*). In Figure 2 an average of 15 SWNTS grow from each 1-μm-diameter dot with lengths ranging from 0.2 to 10 μm. Most of the diameters were $\sim 1.1 \pm 0.1$ nm indicating that they were single-walled nanotubes, while some had diameters of ~2 nm suggesting bundles may be present. For most of the nanotubes in Figure 3A, it was possible to identify nanoparticles attached to their ends. The heights of the attached nanoparticles ranged from 0.9 to 4.2 nm which is a smaller size range than the original nanoparticles (3.8−7.8 nm). This can be explained by realizing that upon heating, spherical particles will wet the surface to form small mounds. For nanoparticles in the range of 3.8−7.8 nm, one would expect the heights to decrease to about 2−5 nm. A few of the attached nanoparticles had diameters >5 nm, but in every instance the height was convoluted with an adjacent taller cluster of nanoparticles, likely making the height measurement in these instances too large. Significantly, early introduction of H_2 dramatically reduced the SWNT yield.

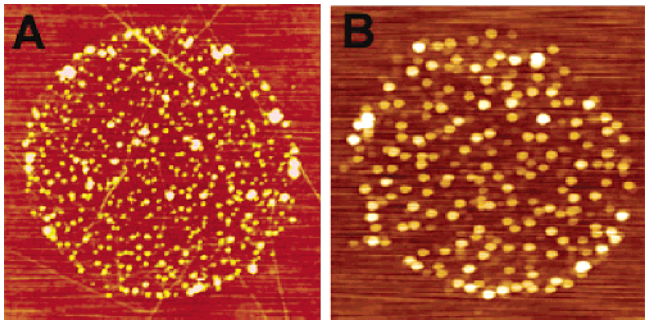

Figure 3. High-resolution images of 1-μm dots of FeNP catalyst after (A) *growth 1* without H_2 pretreatments and (B) *growth 2* with 30 s H_2 pretreatment. There are 17 SWNTs growing from the dot in (A) and none from the dot in (B). The average heights of the nanoparticles within the dots are (A) 4.8 nm and (B) 3.8 nm.

Table 1. Nanoparticle Parameters and Nanotube Yield

sample	nanoparticles per 1-μm dot	nanoparticle dimensions (nm)[a]	SWNT yield per 1-μm dot
before growth	>10 000	H = 5.7 ± 1.8; W = 13−18	
growth 1	1634	H = 4.8 ± 1.5; W = 13−20	15
growth 2	251	H = 3.8 ± 1.2; W = 30−50	<0.1

[a] As measured by AFM, *H* is the height and *W* is the width. Note that *W* is convoluted with the ~15 nm diameter of the probe tip.

By initiating the H_2 flow only 30 s before the CH_4 flow, the yield of SWNTs is reduced to less than 1 SWNT per 10 dots (*growth 2*). Longer lead times can completely suppress the SWNT growth from the FeNP regions. Complete suppression of SWNT growth can also be achieved by allowing the substrate to anneal at 850 °C for an extended period prior to introduction of reactive gases. The results are summarized in Table 1.

Insight into the growth mechanism can be gleaned from AFM images of the catalyst regions before and after growths under different conditions. Height images of a single dot are shown *before growth* (Figure 1B), after high-yield *growth 1* (Figure 3A), and after the no-yield *growth 2* (Figure 3B). Before growth, individual FeNPs can be distinguished and are relatively uniform and moderately packed (Figure 1B). In *growth 2* the particle widths have increased to 30−45 nm indicating that the nanoparticles have fused. After the high-yield *growth 1*, the particle widths of 15 nm are at the resolution of the AFM probe tip, so particle widening cannot be ruled out. However, the particles are no longer well packed and appear to have fused. The AFM of the no-yield growth shows the greatest degree of particle fusion. To quantify the degree of fusing, particle counts were determined for each image since widths less than ~20 nm are highly convoluted with the AFM tips. It was not possible to directly count the particles in Figure 1B. To estimate the particle density *before growth*, a moderately packed monolayer of individual and small aggregates of 5.8-nm particles was assumed in order to calculate a lower bound of ~10 000 particles in the dot. For *growths 1* and *2*, the particles were easily identifiable in the AFM images and were counted directly and listed in Table 1. These particle counts and dimensions are consistent with conservation of total iron mass after sintering.[27] The reduction in nanoparticle counts with

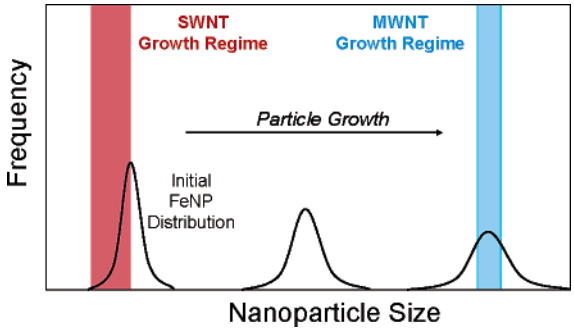

Figure 4. Schematic illustration of FeNP size distribution and nanotube growth. High-temperature treatment causes nanoparticle sintering and an increase in the average nanoparticle size. The initial FeNP size distribution was ideal for growing 1.1-nm-diameter SWNTs at 850 °C in CH_4/H_2 (1500: 50 sccm). Brief H_2 pretreatment accelerated nanoparticle sintering, quickly pushing the FeNP size distribution outside of our growth regime.

concomitant size increases demonstrate that the nanoparticles sinter during the growth process, and that introduction of H_2 before CH_4 (*growth 2*) causes rapid acceleration of the coalescence, probably by reduction of the passivating iron oxide shells to the more mobile Fe species.

The results are consistent with previous research showing that growth of SWNTs from nanoparticles is highly sensitive to growth conditions (gas composition, pressure, and temperature).[11,12,14,19,20] In fact, this notion was our motivation for synthesizing FeNPs with a moderate size distribution (as opposed to a narrow size distribution varying <%10) so as to improve our chances of having particles of the right size for good SWNT growth. In our growths, the initial FeNP distribution had a fraction of FeNPs ideal for nucleating SWNT growth using our growth conditions. Annealing the FeNPs into larger particles, by prolonged heating or preannealing with H_2, pushed the size distribution outside of the growth regime as illustrated in Figure 4. It should be noted that we did not explore how the nanotube growth was affected by changing the carbon precursor or gas composition. Thus, it is reasonable to expect that, under the appropriate conditions, nanotubes would grow from the larger inactive FeNPs that resulted from sintering in our studies. For instance, Cheung found that single and multiwalled nanotubes grew from 9- and 13-nm-diameter iron nanoparticles,[14] whereas in our study, nanotubes grew only from nanoparticles less than 5 nm in diameter. While a full comparison to the results of Cheung is not possible since nanotube yields were not reported, there are some important differences between the two systems. A key difference between our study and that of Cheung is that the larger nanoparticles in our study were formed by sintering, even for the best case of *growth 1*. It is thought that prevention and termination of nanotube growth occurs by overcoating of catalytic nanoparticles with carbon,[11] and this mechanism likely played an important role in our system, where only an average of 15 out of an initial 10 000 particles resulted in nanotubes. It is possible that overcoating occurred on the fused particles before nanotube growth could initiate, sug-

(27) For the particle counts of *growths 1* and *2* and heights of ~5 and 4 nm, respectively, one expects the widths to be ~13 and ~36 nm, respectively, assuming an initial particle count of 10 000 before heating.

gesting that fusing and overcoating is more favorable than nanotube growth. This could also explain why so few FeNPs lead to nanotube growth, since most are consumed in fusing. Another important difference is that we used methane, whereas Cheung used ethylene for most of the growths reported. The fact that ethylene decomposition is more favored than for methane might explain why Cheung observes growth from larger nanoparticles which require more feedstock. However, in one instance, they report growth of double-walled nanotubes from 9-nm nanoparticles using methane as a feedstock. Here comparison is difficult since the exact gas composition was not reported and results of growth from other sized nanoparticles from methane were not reported. Again, the kinetics of overcoating could be significantly different in our closed packed nanoparticle system, thereby preventing nanotube growth from particles >5 nm in diameter.

Our results have important implications for growing single-walled nanotubes from patterned catalysts. The primary motivation for growing nanotubes from monodisperse nanoparticles is to control the nanotube diameter and ultimately its chirality. To date, control over SWNT diameters has been achieved by growing from iron nanoparticles isolated from one another on a substrate. This situation is more difficult to achieve in patterned regions where catalyst is typically concentrated or packed. In this case, our results show that sintering will tend to grow the nanoparticles during heating. To maintain control over SWNT diameters for technological applications, it will be critical to prevent FeNP aggregation. Some possible approaches might use some combination of minimizing high-temperature annealing and reducing conditions (such as H_2 pretreatment), maintaining nanoparticle separation, and immobilizing nanoparticles on the substrate.

Finally, we note that the details of the gas flows in the vicinity of the sample have a large effect on SWNT growth. Initially, we would preanneal in H_2 for $1-2$ min using boat-shaped sample holders with $\sim$1-cm-high lips. The yields from FeNPs varied from 0 to a few SWNTs per 1-μm dot. When we switched to flat sample holders, the SWNT yield from FeNPs was consistently 0 until we stopped preannealing in H_2. To understand this difference, we imaged the gas flows at room temperature using smoke generated from a heated filament soaked with oil. The flat holder allowed laminar flow over the sample, whereas the boat had stagnant re-circulating zones near the lips. The difference in SWNT yield can be explained by the stagnant gas pockets that slow the H_2 from reaching the sample, effectively diminishing the degree of FeNP aggregation. The variation between runs using the boat was a result of differing degrees of gas mixing caused by small changes in sample and boat positioning.

We have demonstrated a reliable method to pattern FeNP monolayers into 200-nm dots on substrates and to grow SWNTs from the patterned regions. The growth of SWNTs from FeNPs is highly sensitive to both the size of the nanoparticles and the gas composition. By characterizing the evolution of FeNP size under different growth conditions, we have determined that it is important to regulate nanoparticle aggregation to have good control over SWNT growth from patterned nanoparticles. Our FeNP patterning method, as well as our SWNT growth model, should be important for developing nanotube-based device technology.

Acknowledgment. The research described in this paper was carried out at the Jet Propulsion Laboratory, California Institute of Technology, and was sponsored by the DARPA NMASP program, the NASA Code R/T BioNano program, and the National Aeronautics and Space Administration.

CM048795M